Internal cooling of a gas turbine blade using Ranque-Hilsch vortex flow

Daisy Galeana[a], Ashenafi Abebe[b], and Asfaw Beyene[c]

[a] Solar Turbine Inc., San Diego CA, USA, Galeana_Daisy@solarturbines.com
[b] Debre Berhan University, Debre Berhan, Ethiopia, abebeashenafi7@gmail.com
[c] Department of Mechanical Engineering, San Diego State University, San Diego CA, USA, abeyene@sdsu.edu

Abstract:

Efficiency of a gas turbine engine is directly impacted by the turbine inlet temperature and the corresponding pressure ratio. A major strategy, aside from use of costly high-temperature blade materials, is increasing the turbine inlet temperature by internally cooling the blades using pressurized air from the engine compressor. Understanding the fluid mechanics and heat transfer of internal blade cooling is therefore, of paramount importance for increasing the temperature threshold, hence increasing engine efficiency. This paper presents results of a novel cooling approach, i.e., the use of Ranque-Hilsch vortex flow for first row gas turbine blade cooling. Test results clearly demonstrate the successful formation of continuous Ranque-Hilsch vortex flow by injecting compressed air into a cylindrical chamber equipped with seven air inlets. Separated boundaries of the reversed flow with detectable boundaries were accompanied by a significant drop in temperature on the cold stream side. At inlet pressure of 63 kPa, the outlet temperature from the vortex tube dropped below 0°C, which allowed blade temperature drop of about 200 °C. The thermal efficiency of the gas turbine increased from 40% to 43% by vortex-cooling the blades with 10% mass of compressed air extracted at about 910 kPa. For the tested scenario of a 17 MW engine, the partial extraction had a better efficiency increment than extraction at full compression which was 1200 kPa.

Keywords:

Thermodynamics; Gas turbine engine, internal blade cooling, thermal efficiency, power output, Ranque-Hilsch vortex flow, experiment.

1. Introduction

The life cycle of a gas turbine engine blade is most affected by high the operating temperature, constant centripetal loading, and thermally induced stresses, particularly during start-up and shutdown. The thermal efficiency of the engine increases with the increase of the pressure ratio and the firing temperature which increases the turbine rotor inlet temperature (TRIT). As the firing temperature increases, the heat transferred to the turbine also increases, rising above the material temperature threshold which requires mitigation measures of material failure if upholding the high temperature is desired to maintain high efficiency. This requires internal cooling of the rotor blades. Significant research has been going on for decades to design an internal cooling system particularly for the first-stage blades, to achieve higher firing temperature. Effective internal cooling of the rotating blades is a significant challenge, compounded by wake-induced turbulence and unfavorable area ratios between inner and outer surfaces [1] [2]. This can cause formidable challenges to turbine internal cooling.

Various cooling techniques are applied on the turbine blade to keep the working temperature within a safety limit [3] [4] [5]. It is a common practice to cool high-pressure turbine blades using air from the compressor which is routed through the turbine blades thereby lowering its temperature. Swirl cooling is one of the many techniques used for such cooling. The idea is to route swirling air from the compressor through the turbine blade's internal passages [6]. The first rows of turbine blades typically operate at a temperature that exceeds 1,200 °C [7] [8] [9], and therefore, may greatly benefit from internal cooling if higher firing temperature is to be entertained.

Analytical and experimental modeling in the leading-edge area of the blade, with regard to internal swirl cooling systems, could result in optimization of turbine blade designs with respect to heat transfer, cost, and performance, as well as reduced downtime [10] [11] [12]. Adding complexity to the demanding task of managing high temperature without its accompanying penalties is the driving desire for a long-term life cycle without frequent inspections and overhauls. Turbine blades withstanding high temperatures and constant mechanical stresses, which limit the turbine blade life cycle, may also cause permanent material deformation

https://doi.org/10.52202/069564-0007

[13] [14]. These can also cause local plastic yielding while contributing to material creep [15]. Some innovative techniques have been proposed to improve the convective heat transfer for internal cooling of gas turbine airfoils, including rib turbulators, pin fins, dimpled surfaces, impingement cooling, and swirl flow cooling [16] [17] [18] [19] [20].

Of particular interest here, the topic of our research, is “swirl cooling” which induces a reverse flow. One such innovative approach is discussed by Glezer et al. [14] who present experimental results comparing three separate studies. The research provided a better understanding of the screw-shaped swirl cooling technique for heat transfer in internal swirl flow, where heated walls were applied and a screw-shaped cooling swirl was generated, introducing flow through discrete tangential slots. The authors mention that the Coriolis forces play an important role in enhancing the internal heat transfer when their direction coincides with a tangential velocity vector of the swirl flow.

Another paper on the same subject of swirl cooling, [21] states that the local surface Nusselt numbers increase when increasing the Re number (the range in this study was from 6,000 to about 20,000). As a result, the local swirl chamber heat transfer and flow structure are linked to increased advection as well as notable alterations to vortex behavior near the concave surfaces of the swirl chamber. One key result was that, along with the Nusselt number, the changes of surface heat transfer downstream of each inlet increased sharply when compared to other locations. Hedlund et al. [21] observe that as the turbulent flow becomes more pronounced, the axial and circumferential velocities get larger and intensify the turning of the flow from each inlet.

Other studies show that blade internal swirl cooling is effective and can afford long term life to blades especially if employed in tandem with advanced blade alloys [22] [23]. Experiments conducted by Ligrani et al. [3], Moon et al. [1], and Glezer et al. [13] introduced an internal cooling structure as one way to attend to high temperature management in gas turbine cooling, Fig. 1.

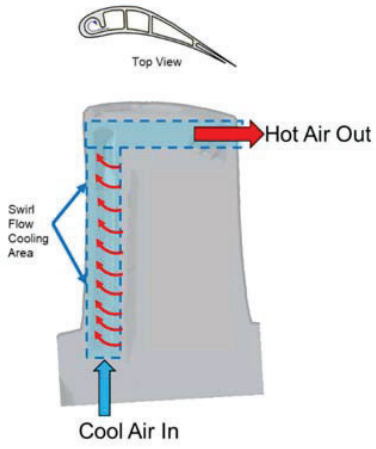

Figure 1: Turbine blade leading edge internal cooling design, [4].

The above summaries of recent developments in turbine blade internal cooling show advances in several fronts. However, the idea of applying the Ranque-Hilsch vortex flow for internal blade cooling has never been investigated. Thus, the focus of this study is to conclusively prove that sustained reverse flow with accompanying temperature drop can be produced, which allows the use of the cold stream for a gas turbine blade internal cooling. The vortex flow is injected tangentially through holes to induce the vortices, as shown in Fig. 2.

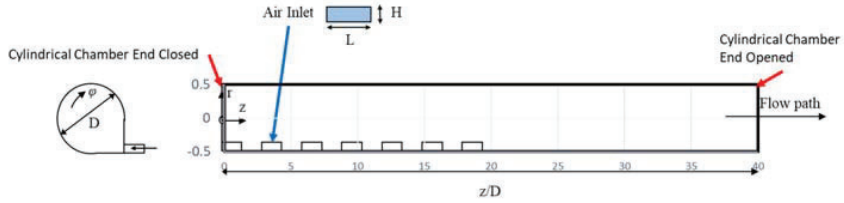

Figure 2: Cylindrical chamber geometry with seven air inlets, [24].

https://doi.org/10.52202/069564-0007

2. Experimental setup

The main piece of the lab setup for the vortex flow cooling experiment is LaVision Stereo-PIV system, which includes a LaVision PC, two ImagerproX cameras, two Nd-YAG lasers, and LaVision particle seeder as shown in Fig. 3. The cameras are mounted on a stand equipped with stepper motors, allowing it to travel freely along the chamber length. The fluid is seeded with olive oil particles that have diameters in the range of 1-3 μm and specific gravity of 0.703. These oil tracer particles are chosen because they are small enough that they have little inertia; validating the tracer particle motion best reflects the actual flow path. The seeding particles in the fluid distribute the laser light, which is captured by the video acquisition system. The Nd-YAG laser is a Pegasus PIV with a wavelength of 527 nm and maximum energy of 20 mJ per pulse. The Nd-YAG laser serves as the illumination source for the PIV system and is manipulated through the appropriate use of optical instruments to produce a laser sheet of 2 mm thickness on the chamber's bottom wall. This setup allows the illumination of planes parallel to the vertical axis. Two high-speed and high-resolution CCD cameras (Phantom v7.3. 800_600 pixels, 12 bit) capture images of the illuminated PIV particles at a rate of 100 frames per second. With that frame rate, 2000 images are acquired over a period of 10 seconds, similar to the measurement duration in the experiment conducted by others [12-13].

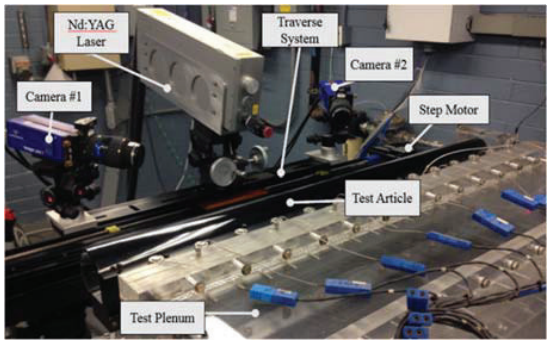

Figure 3: Hardware setup.

DaVis is utilized to collect PIV data, all data points are taken and collected in one file set which exports time-average velocity and is post-processed in DaVis to be transferred into MATLAB. MATLAB cleans up DaVis raw data and allows the calculation of crucial flow field variables. All velocity calculations are conducted in MATLAB, followed by a file structure that prepares data for visualization in Tecplot 360, which is used for data visualization. One advantage of using Tecplot 360 is that it provides powerful flow visualization options. Created some macros to automate visualization procedures. To create smooth transitions in between data points, a data interpolation scheme was employed.

3. Generating a Ranque-Hilsch vortex flow

Before committing to the use of the cold stream of the Ranque-Hilsch flow, it would behoove us to first scrutinize its occurrence within the theoretical scope presented above, with an accompanying temperature drop - significant enough to cool the gas turbine blades.

3.1. Theoretical justification, Navier Stokes Eq. and CFD

The Navier-Stokes, centrifugal force, and centrifugal velocity equations can be used to show prevalence of the reverse flow in the cylindrical chamber. Once preliminary values were entered, the results show a radial pressure drop of about 140 Pa, which spans from the gauge pressure at the inlet of approximately 340 Pa, as clearly illustrated in Fig. 4.

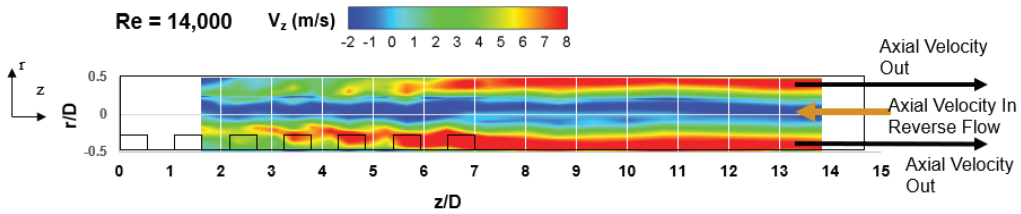

Figure 4: Radial pressure drop estimate.

https://doi.org/10.52202/069564-0007

CFD simulations can further lay evidence to predict the loadings and flow distributions of blade rows, including for end-wall regions. As a tool, CFD can produce valuable outputs, albeit its limitations in predicting turbine heat transfer, mainly because of constraints in modeling turbulence and vortices, uncertainty of boundary conditions, and the inherent flow unsteadiness in turbomachinery. Here we simulate velocity, temperature, and pressure distributions to show if their profiles support the notion of existence of a reverse flow, and if the continuity equation is satisfied.

Velocity: The velocity streamline for the entire fluid domain is presented in **Error! Reference source not found.**5. The largest velocity value is noticed at inlet 7 at 30.457 m/s. There are three reversed flow cases at the inlets 1, 2 and 3. The velocity is minimum near the end of the chamber.

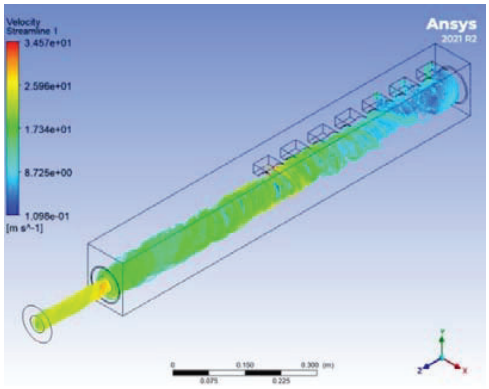

Figure 5: Velocity streamline of the fluid domain.

Temperature and Pressure: The temperature and pressure distribution along the cylindrical chamber are given in Fig. 6. The highest pressure is observed in front of inlet seven reading 979 Pa. However, after air inlet seven the cross-section of the chamber, the pressure distribution shows significant drop resulting in -30.870 Pa. The temperature contour indicates separated cold and hot streams. These temperature and pressure show existence of a reverse flow with a temperature drop.

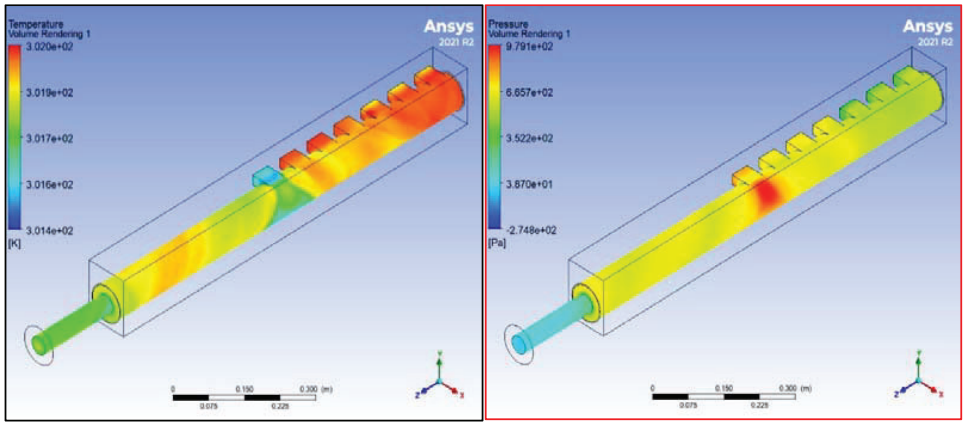

(a) (b)

Figure 6: Temperature (a) and pressure (b) contour of the vortex chamber and tube

Continuity Eq.: To confirm the mass is balanced, we assess the mass flow rate at some distance "z" downstream of the flow. The goal here is to plot the mass flow rate at the three assumed Re numbers to confirm that the mass flow rate going into the cylindrical chamber matches the total mass flow rate going out of the chamber as cold and hot streams. Figure 7 shows that the mass flow rate going into the chamber matches the sum of reversed and unreversed flows leaving the chamber, which proves the reverse vortex flow takes place inside the cylindrical chamber.

https://doi.org/10.52202/069564-0007

The total mass inflow rate through the system is 0.0535 kg/s. This is also the sum of the flow rate through each inlet, which again is the same as the flow rate at the outlet, as shown in Tab 2.

Table 2: Summary of mass flow rate at the inlets and outlets.

Location	Inlet 1	Inlet 2	Inlet 3	Inlet 4	Inlet 5	Inlet 6	Inlet 7	Outlet
Flow Rate, kg/s	-0.0085	-0.0088	-0.0075	0.0096	0.0033	0.0063	0.0343	0.0287

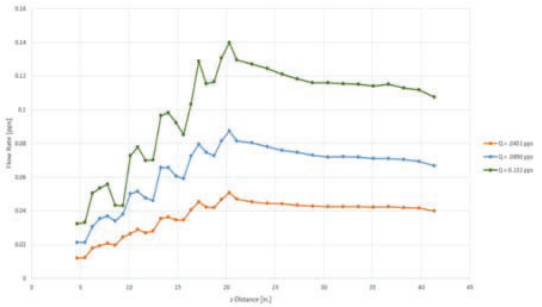

Figure 7: Mass flow rate vs. z-Distance at all three Re numbers of cylindrical chamber.

4. Evidence of prevalence of reverse flow

4.1. Thermochromic Liquid Crystal (TLC)

The cylindrical chamber is made of clear acrylic material, painted with TLC to allow visualization of color changes within the required time range. As the air enters the plenum, Fig. 8, it passes into a rectangular heating mesh, leading to rectangular cross-sectional air inlets with individual hydraulic diameters (D_H) of 0.011 m. These inlets are connected to the principal vortex chamber so that one surface is tangent to the chamber inner circumference.

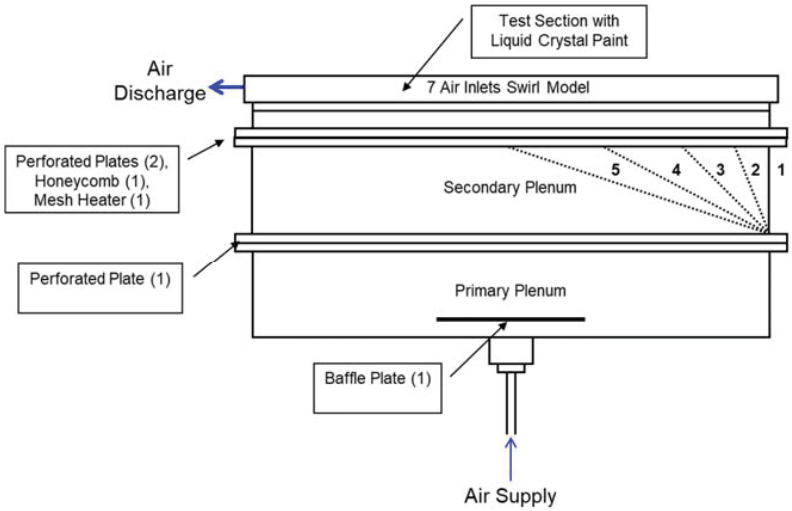

Figure 8: TLC painted test stand with plenums attached.

The surface area optics suitable for the spatial resolution are painted, first the cylindrical chamber is coated with liquid crystal paint, followed by black paint. A coupon is built, following the same process for calibration purposes, coated with liquid crystal paint, and followed by black paint.

TLC Data Collection: An in-house software is used to synchronize the entire liquid crystal experiment. The data is collected by continuously polling after the system is heat-soaked to the required temperature. The data acquisition step size is 0.5 seconds and the VXI is set to a time interval of 0.2 seconds. The video file is converted to an AVI file, imported into the "Liquid Crystal Image Analyzer (LCIA)," as shown in Fig. 9. Contact resistance and temperature drop through the wall are determined experimentally from the calibration process

https://doi.org/10.52202/069564-0007

and green time is measured simultaneously. Using seven calibrated thermocouples equally separated across the length of the cylindrical chamber, the temperature of the air entering the cylindrical chamber is measured. All measurements are collected when the cylindrical chamber is at steady state and when the heating mesh on the plenum reaches 35°C.

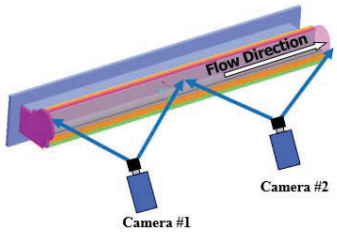

Figure 9: heat transfer data collection by two cameras for the painted test stand.

Once the green time image is calculated, then the probe locations are associated with columns of temperature readings in the temperature probe data file. Noise is edited out with an eraser image mask, followed by the region of interest definition using a polygon mask. These final images are then exported as JPEG image files. Cameras recording in DV format are set up to view the liquid crystal coated surface of the test stand, capturing 10 samples per second. The air flow rate is set as the liquid crystal transitions at 35°C and regulator pressure at 6.89 KPa. Once the system is heat soaked, cameras start recording. When the paint has fully transitioned to blue, the cameras and data acquisition system are stopped manually.

The data points were taken at 33 locations at a distance of 19.81 mm from each other, as shown in Figure 10 and Fig. 11. Data were collected at both locations, in between air inlets and at the middle of the air inlets (i.e., data point #2 and data point #4, respectively) to show the complicated flow and its variation.

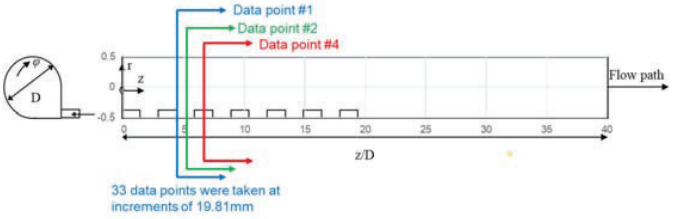

Figure 10: Data point locations in increments of 19.81 mm.

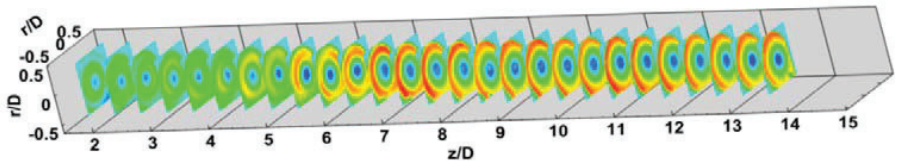

Figure 11: Cross-sectional area of data points.

4.1.1. Axial Velocity Distribution

As the Re number increases, the axial velocity, V_Z, intensifies, measuring higher on the outer wall region, as shown in Figure 12. From upstream to downstream, the V_Z ranges from -2 to 7 m/s in all three Re numbers, as is expected in a cylindrical chamber. The outer wall region velocity increases across the length, reaching a maximum velocity at the second half of the vortex chamber. Another observation is the high V_Z in the direction of the outer wall region. Between the core and the chamber wall in the outer wall region, an inertia-driven vortex was observed and measured a flow field pattern that is critically different between high to low Re numbers.

https://doi.org/10.52202/069564-0007

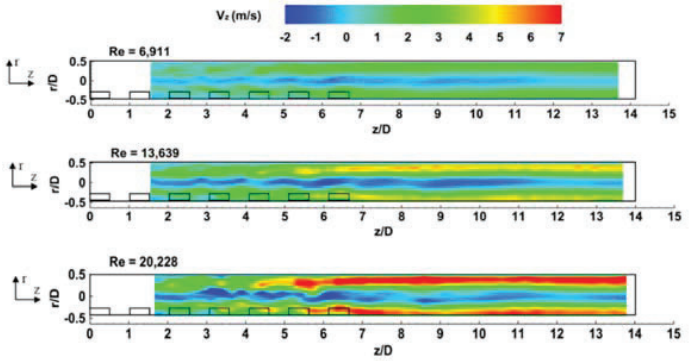

Figure 12: Axial velocity distribution of cylindrical chamber at all three Re numbers.

4.1.2. Reverse Vortex Flow at the Center of the Cylindrical Chamber

With this geometry, the vortex flow cooling has important axial and circumferential components of velocity, and the overall flow pattern through the cylindrical chamber behaves similar to a vortex tube, also known as the Ranque-Hilsch vortex tube, a mechanical device that separates a compressed air into hot and cold streams with temperature difference reaching over 250°C. Although unintended, the detailed flow behavior inside a Ranque-Hilsch vortex tube and flow reversal in the cylindrical chamber share similitudes. The velocity profile was measured for both air and water operated Ranque-Hilsch vortex tube. Based on this study, there was a remarkable agreement between theoretical estimation and experimental results. Furthermore, the unintended consequence of the vortex flow behavior needed more analysis; utilizing 3-D stereo-PIV at the nominal Re = 13,639, three cross-sectional areas were chosen. **Error! Reference source not found.** 10 shows the three cross-sectional areas z/D = 3, 6, and 13 carefully studied looking for evidence of the reverse flow and captured it and all three cross-sectional areas to show reverse flow. Stereo-PIV is a powerful tool able to capture in great detail how each droplet behaves and map the axial velocity field flow. The discovery of this unintended behavior is so astronomically important that more research and analysis had to be completed to satisfy the minds of the experts. The next step is to understand the vortex flow behavior where the reverse flow exists.

Figure 13 presents the normalized axial velocity against the cylindrical chamber length, downstream of the flow. The pressure decreases downstream on the outer chamber wall, the reverse flow at the centerline is increasingly visible.

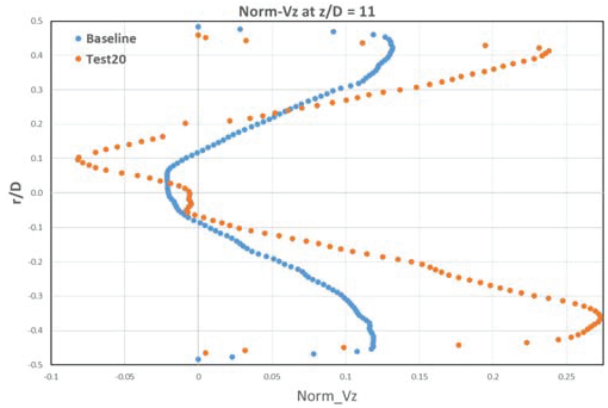

Figure 13: Normalized V_z at z/D = 11 of cylindrical chamber.

4.2 Video Evidence

In addition to the above listed techniques, the existence of a reverse flow was also validated using a video. For this purpose, we prepared a wire with a piece of light string, rag attached at the end of the wire. The wire is then inserted at three different locations to see its motion. The string moved in the direction of the flow in all the three locations. The string changes direction as it is moved across the internal boundary of the reversed flow.

https://doi.org/10.52202/069564-0007

Figure 14: Video evidence of the reverse vortex flow using a wire and a soft yarn attached.

5. Conclusion

The results show that for an incoming air of 100kPa, the temperature and pressure drops are significant. The exit temperature depends on the input pressure with a nearly linear relationship. As the input pressure increases, the outlet temperature of the cold stream decreases. For validation purposes, the compressed air temperature at inlet was kept constant at a value of 28°C for the simulation. When the air at 1kPa was admitted to the vortex chamber, the exit temperature remained the same for both the simulation and the experimental test. However, at 63kPa inlet pressure, the stream temperature cooled to 0°C i.e., yielding a temperature drop of about 29°C.

Experimental data collected from the cylindrical vortex chamber which models internal cooling passage of a blade located near the leading edge of a gas turbine blade, for Re range of 7,000 to 21,000 show outstanding accuracy and 3-D resolution obtained with the Stereo-PIV imaging techniques employed here. The combination of CFD and experimental data reveal distinct advantages of the vortex cooling concept introduced here, over other cooling methods.

The versatility of the vortex cooling design to redistribute a different path of heat load profile without major casting changes was demonstrated by using seven air inlets. The span of the outer-wall velocity flow fields increases, due to the enlargement of the vortex flow core. The TLC heat transfer test results exemplify how the Nu were measured favourably at the middle length of the chamber and values decline downstream.

The primary objective of this research has been met by performing tests to prove prevalence of a reverse flow in the swirl chamber. The channel served as a Ranque-Hilsch vortex tube. As a result, the compressed air was separated into hot and cold streams with temperature difference reaching over 250°C. The detailed flow behaviour inside a Ranque-Hilsch vortex tube and flow reversal in the cylindrical chamber share similarities. Based on this study there was an impressive and conclusive presence of reverse axial flow at the core as illustrated in the experimental results. Simulation results correlated the experiment results and validated the reverse flow with similar mass flow rate and pressure gradients of 0.0535 kg/s and 979 Pa, respectively. The CFD recreated the reverse flow at Re = 14,000. The results affirm that higher pressure input can contribute to lowering the temperature at the exit from the chamber, favouring the cooling process. The thermal efficiency increased by about 3% when the blade is cooled by extracting 10% partially compressed air. This is a significant gain.

Nomenclature

D	Circular chamber diameter, m
D_H	Hydraulic diameter of one swirl chamber inlet, m
Q	Mass flow rate, kg/s
H	Height, m
k	Turbulent kinetic energy, m^2/s^2
L	Cylindrical chamber length, m
P	Pressure, Pa
R	Radial distance measured from chamber centreline, m
Re	Reynolds number
r	Radial distance, m
S_N	Swirl number
V_z	Axial velocity, m/s
V_ϕ	Circumferential velocity, rad/s
W	Air inlet width, m
r, θ, z	Cylindrical coordinates
ρ	Density, kg/m^3
v	Kinematic viscosity, m^2/s
$\delta_f = m_f/m_a$	Mass of fuel to mass of air ratio
P_{ra}	Pressure ratio at the point of extraction
T	Temperature, K
η	Efficiency

https://doi.org/10.52202/069564-0007

Subscripts and superscript

a	Air
f	Fuel
CA	Cooling air fraction
t	Turbine
c	Compressor
‘	Ideal compression/expansion process

References

[1] Moon, H.K., O'Connell, T., and Glezer, B., "Heat Transfer Enhancement in a Circular Channel Using Lenghtwise Continuous Tangential Injection," *Heat Transfer,* vol. 6, pp. 559-564, 23-28 August 1998.

[2] Moon, H.K., O'Connell, T., and Glezer, B., "Channel Height Effect on Heat Transfer and Friction in a Dimpled Passage," *Journal of Engineering for Gas Turbines and Power, ASME,* vol. 122, pp. 307-313, 2000.

[3] Ligrani, P., "Heat Transfer Augmentation Technologies for Internal Cooling of Turbine Components of Gas Turbine Engines," *International Journal of Rotating Machinery,* vol. 1, pp. 1-33, 2013.

[4] Ligrani, P., Goodro, M., Fox, M., and Moon, H.-K., "Full-Coverage Film Cooling: Film Effectiveness and Heat Transfer Coefficients for Dense Hole Arrays at Different Hole Angles, Contraction Ratios, and Blowing Ratios," *Journal of Heat Transfer, ASME,* pp. 031707-1 - 031707-14, 2013.

[5] Ligrani, P., Goodro, M., Fox, M.D., and Moon, H.-K, "Full-Coverage Film Cooling: Heat Transfer Coefficients and Film Effectiveness for a Sparse Hole Array at Different Blowing Ratios and Contraction Ratios," *Journal of Heat Transfer, ASME,* vol. 137, pp. 032201-1 - 032201-12, 2015.

[6] Kumar, S. and Singh, O., "Thermodynamic Evaluation of Different Gas Turbine Blade Cooling Techniques," *Thermal Issues in Emerging Technologies,* pp. 237-244, 2008.

[7] Kurz, R., "Gas Turbines Performance," *Proceedings of the Thirty-Fourth Turbomachinery Symposium,* pp. 131-145, 2005.

[8] Gao, Z., Narzary, D.P., and Han, J.-H., "Film Cooling on a Gas Turbine Blade Pressure Side or Suction Side with Axial Shaped Holes," *International Journal of Heat and Mass Transfer,* vol. 51, pp. 2139-2152, 2008.

[9] Garg, V. and Gaugler, R., "Effect of Coolant Temperature and Mass Flow on Film Cooling of Turbine Blades," *International Journal of Heat and Mass Transfer,* vol. 40, no. 2, pp. 435-445, 1997.

[10] Kusterer, K., Lin, G., Bohn, D., Sugimoto, T., Tanaka, R., and Kazari, M., "Leading Edge Cooling of a Gas Turbine Blade with Double Swirl Chambers," *Proceedings of ASME Turbo Expo 2014: Turbine Technical Conference and Exposition,* pp. 1-11, 2014.

[11] Ahn, J., Schobeiri, M.T., han, J.-C., and Moon, H.-K., "Effect of Rotation on Leading Edge Region Film Cooling of a Gas Turbine Blade with Three Rows of Film Cooling Holes," *International Journal of Heat and Mass Transfer,* vol. 50, pp. 15-25, 2007.

[12] Chung, H., Park, J.S., Sohn, H.-S., Rhee, D.-H., and Cho, H.H., "Trailing Edge Cooling of a Gas Turbine Blade with Perforated Blockages with Inclined Holes," *International Journal of Heat and Mass Transfer,* vol. 73, pp. 9-20, 2014.

[13] Glezer, B., Moon, H.K., and O'Connell, T., "A Novel Technique for The Internal Blade Cooling," *The American Society of Mechanical Engineers,* pp. 1-10, 10-13 June 1996.

[14] Glezer, B., Moon, H.K., Kerrebrock, J., Bons, J., and Guenette, G., "Heat Transfer in a Rotating Radial Channel with Swirling Internal Flow," *ASME,* pp. 1-7, 1998.

[15] Han, J.-C., and Chen, H.-C., "Turbine Blade Internal Cooling Passages with Rib Turbulators," *Journal of Propulsion and Power,* vol. 22, no. 2, pp. 226-248, 2006.

[16] Ligrani, P.M., Hedlund, C.R., Babinchak, B.T., Thambu, R., Moon, H.-K., and Glezer, B., "Flow Phenomena in Swirl Chambers," *Experiments in Fluids,* vol. 24, pp. 254-264, 1998.

https://doi.org/10.52202/069564-0007

[17] Ligrani, P.M., Choi, S., Schallert, A.R., and Skogerboe, P., "Effects of Dean Vortex Pairs on Surface Heat Transfer in Curved Channel Flow," *Internationl Journal of Heat and Mass Transfer,* vol. 39, no. 1, pp. 27-37, 1996.

[18] Ligrani, P.M., Mahmood, G.I., Harrison, J.L., Clayton, C.M., and Nelson, D.L., "Flow Structure and Local Nusselt Number Variations in a Channel with Dimples and Protrusions on Opposite Walls," *International Journal of Heat and Mass Transfer,* vol. 44, pp. 4413-4425, 2001.

[19] Ligrani, P.M., Oliveira, M.M., and Blaskovich, T., "Comparison of Heat Transfer Augmentation Techniques," *AIAA JOURNAL,* vol. 41, no. 3, pp. 1-26, March 2003.

[20] Li, S.-J., Lee, J., Han, J.-C., Zhang, L., and Moon, H.-K., "Turbine Platform Cooling and Blade Suction Surface Phantom Cooling from Simulated Swirl Purge Flow," *Journal of Turbomachinery,* vol. 138, pp. 1-11, 2016.

[21] Hedlund, C.R. and Ligrani, P.M., "Local Swirl Chamber Heat Transfer and Flow Structure at Different Reynolds Numbers," *Journal of Turbomachinary,* vol. 122, pp. 374-385, April 2000.

[22] Nasir, H., "Turbine Blade Tip Cooling and Heat Transfer," Doctoral Dissertation, *Louisiana State University,* 2004.

[23] Morris, W.D. and Chang, S.W., "An Experimental Study of Heat Transfer in a Simulated Turbine Blade Cooling Passage," *International Journal of Heat and Mass Transfer,* vol. 40, no. 15, pp. 3703-3716, 1997.

[24] Mebrat A.A., Galeana D., and Beyene A., "Vortex cooling of a gas turbine blade: comparison of single and bidirectional swirl formation," *Proceedings of ECOS 2022 - The 35rth International Conference on Efficiency, Cost, Optimization, Simulation and Environment,* 2022.

https://doi.org/10.52202/069564-0007